Temperature-dependent Resonant Raman Scattering of Yttria Doped Zirconia Phases in Thermal Barrier Coatings

Samuel Margueron[1], Ausrine Bartasyte[1,2]

[1] FEMTO-ST Institute, CNRS (UMR 6174) - Université de Franche-Comté, ENSMM, 26 rue de l'Epitaphe, 25030 Besançon, France

[2] Institut Universitaire de France (IUF)

Abstract

To understand the strong Raman scattering intensity of metastable t'-YSZ thermal barrier coatings, about three times than other phases of yttria doped zirconia, a careful investigation of high temperature phase is performed by ultraviolet Raman scattering at 355 nm up to 1500 °C. The studied specimens are thermal barrier coating as well as single crystals of monoclinic zirconia and cubic yttria stabilized zirconia. The ultraviolet Raman scattering efficiency of cubic and metastable zirconia indicate a crossover between the laser line and the band gap of these phases that are well explained by Loudon's resonant Raman scattering model. In the case of pure zirconia, the Raman scattering intensity presents a tetragonal martensitic phase transition at around 1050–1200°C with a small anomaly of Raman intensity. From this study, one can infer that the strong Raman scattering intensity of t'-YSZ may originate from the photoelasticity effect of the ferroelastic phase.

Keywords: thermal barrier coatings, yttria stabilized zirconia, resonant Raman scattering

1. Introduction

Yttria stabilized zirconia Y_2O_3-ZrO_2 (YSZ) is highly applied material as high temperature thermal barrier coatings (TBC) [miller1997], electrodes in solid oxide fuel cells (SOFC) [ikeda1985], [vladislav1999] or bioceramics [Heimann2015]. The phase diagram of YSZ solid solutions [scott1975], [chevalier2009] has been intensively studied in relation to the thermal conductivity [mevrel2004], the strength [garvie1975] and the lifetime of TBC [scott1975], [miller1997], [evans2008], [chevalier2009] and ionic conductivity [vladislav1999], [ngai2013].

YSZ presents several polymorphs with monoclinic, tetragonal, and cubic structures. The monoclinic phase (m-ZrO_2) of undoped ZrO_2 is stable below 1170 °C while the tetragonal phase structure (t-ZrO_2) occurs between 1170 °C and 2370 °C and the cubic phase (c-ZrO_2) occurs for higher temperature through the melting point (2706 °C). The tetragonal (t-YSZ) and cubic (c-YSZ) transformation can be lowered with alloying with aliovalent ions such as Y_2O_3. Moreover, a metastable tetragonal t' phase (t'-YSZ) [ishizawa1986], widely used in TBC [chevalier2009], has been obtained by the electron-beam deposition of 3–8 wt% of Y_2O_3 from

the quenching of the high temperature tetragonal phase. A peculiar attention has been paid to the monoclinic – tetragonal martensitic phase transition [ishigame1977], [perry1990] as it plays a detrimental role in the degradation and aging of TBC [chevalier2009]. The corrosion of molten salt [miller1997], [evans2008], [Morelli2020] has also become a major concern of TBC lifetime and may be related to high temperature surface reactivity of YSZ, which degrades t' phase.

Raman scattering has been used for studies of the composition, the phase stability, the residual stresses, the temperature behaviour of phonon modes and as an in-situ monitoring in YSZ and TBC [ishigame1977], [feinberg1980], [clarke1982], [perry1990], [cai1995], [lughi2005], [Zhu2020], [cai2020]. In general, the temperature effect induces a decrease of the vibrational frequencies due to the lattice thermal expansion and the anharmonicity of lattice vibration potential induced by the increased phonon population [lughi2007]. The damping of phonons is related to the anharmonicity of the phonon-phonon scattering [lughi2007] but also depends on the chemical disorder [lughi2005], [gouadec2007]. Thus, an in-situ Raman study of TBC corrosion at high temperature is of special interest to analyse Raman phases and intensities. However, the quantitative phase compositional analysis by means of Raman spectroscopy requires the calibration of Raman intensities [clarke1982]. According to off-resonance quantum theory of Raman scattering (with excitation energy below the optical gap), the first order Stokes Raman intensity, I, is given by [perry1990], [fukatsu2010]:

$$I(\omega_{ph}) = A(\lambda_{LASER})\{n(\omega_{ph}, T) + 1\}R(\omega_{ph}) \quad (1)$$

Where $n(\omega_{ph}, T) = 1/\left(e(\frac{\hbar\omega_{ph}}{k_B T}) - 1\right)$ is the Bose-Einstein thermal population factor, ω_{ph} - the angular frequency of phonon, k_B – the Boltzmann constant, T – the temperature, $R\ (\omega_{ph})$ - the Raman gain depending on polarization of the incident and scattered light, and $A(\lambda_{LASER})$ is a factor which takes into account the optical excitation and collection probe system at the laser excitation wavelength, λ_{LASER}. According to Equation 1, and neglecting absorption, the intensity of the first order Raman modes changes with temperature following the factor of Bose-Einstein phonon population. Temperature dependence of Raman intensity of ZrO_2 with visible excitation (with pulse mode) has been reported up to 1400 °C [ishigame1977], [perry1990], whereas, the Raman intensity, measured using visible excitation, decreases as a function of temperature in YSZ [feinber1980], [cai1995]. These results suggest that some absorption may have occurred at high temperature. Moreover, the gain term, $R\ (\omega_{ph})$, of Equation 1 might change with temperature due to the structural changes, thermal expansion, shrinking of the band gap, etc. So far, the temperature change of Raman intensity of YSZ and its relation to the composition/structure/defects and absorption remain not well studied and understood.

The aim of this paper was to relate the Raman intensity to the composition and structure in order to understand the anomalous intensity of t'-YSZ as compared to other phases. For this purpose, we have done characterization of the high temperature phase of tetragonal undoped ZrO_2 in comparison with t' phase at room temperature. To limit thermal background emission at high temperature, excitation with ultraviolet laser (355 nm/3.49 eV) was used to measure the Raman scattering intensity of YSZ systems. The ultraviolet laser line was initially chosen to be

sufficiently far from the gap absorption. However, the Raman spectra at high temperature presented resonance effect, which was not observed at room temperature. The resonance effect was studied by applying Loudon's theory of resonance. It showed that the anomalous intensity of tetragonal t'-YSZ, observed at all Raman excitations, was not related to a resonance effect, but, most probably to the photoelasticity of this ferroelastic phase.

2. Experimental Details

Unoriented (twinned) single crystals of monoclinic zirconia (noted m-ZrO_2) and single crystal of cubic zirconia with 38 wt% of Y_2O_3 doped ZrO_2 (noted 38%YSZ) were provided by Zirmat Corp. (North Billerica [mevrel2004]). Cubic (111) oriented wafer with 19.4 wt% of Y_2O_3 (noted YSZ(111)) was purchased from MTI (Richmond, CA). The composition of the studied samples, determined by X-ray fluorescence, is given in Table I. The samples were optically thinned to about 200 µm. The thermal barrier coating of t'-YSZ with 8.8 wt% of Y_2O_3 (also called TBC) was grown by electron beam physical vapour deposition (EB-PVD) on alumina ceramic substrate and annealed for 24 h at 1000 °C. The TBC coating was later pilled apart from the substrate by manually pressing with a diamond tip to have a flake with a thickness of 200 µm.

Raman spectra were collected in backscattering geometry by using a T64000 UV micro-spectrometer (Horiba, Jobin-Yvon, France). The ultraviolet excitation at 355 nm (3.49 eV) with a maximum power on the sample of 13 mW was generated by an optically pumped semiconductor laser (Genesis, Coherent Inc). The backscattered laser line was suppressed by a notch filter and depolarized before entering the third stage of the T64000 spectrometer with a UV 2400 mm^{-1} grating. The laser was focused with a x20 Near Ultraviolet Mitutoyo objective with a long working distance (LWD). The lateral resolution was around 10 µm. The spectral resolution was about 2 cm^{-1} in the range of 100 cm^{-1} to 1100 cm^{-1}. Additional Raman scattering was done at 532 nm with x50 LWD Olympus objective and appropriate optical filters.

Ultraviolet temperature Raman measurements have been carried out from room temperature (RT) to 1500 °C using a commercial LTS1500 water-cooled heating stage (Linkam Scientific Instruments Ltd) as shown in Figure 1a [margueron2014]. The temperature was stabilized for at least 5 min before each measurement point. The optical windows were replaced by sapphire windows which were checked not to present the absorption of the ultraviolet wavelengths up to 1500 °C. Above 1000 °C, the strong thermal emission background was evaluated by collecting the spectra in the same experimental conditions (time, focus) but without the laser excitation source and removed by direct subtraction from the spectra. To avoid the saturation of CCD due to blackbody radiation emission at temperatures above 1400 °C the acquisition time was reduced but the number of acquisitions was increased accordingly: instead of acquiring for 20 s, we run 4 measurements of 5 s or 2 measurements of 10s. Then, the Raman intensity (number of counts by pixel) was normalized to the acquisition time to be comparable. The intensities of measured spectra were normalized with respect to laser power as well as.

The photoluminescence (PL) in the range of 400 nm to 700 nm of specimens was recorded with the same experimental set-up as Raman spectra but using a 300 mm^{-1} grating. Acquisition times for PL spectra were 0.5 s for m-ZrO_2 and 30 s for other samples. The PL intensity was normalized with respect to the acquisition time, as well. Additional, room temperature measurements were carried on using a 266 nm (4.66 eV) microchip laser (TeemPhotonics) with

deep ultraviolet x40 objective (OFR). This optical system cannot detect emission below 325 nm.

The transmission of 355 nm laser line at different temperatures was measured by redirecting the UV laser through UV resistant optical fibre under the heating stage and by recording the transmitted laser line without a notch filter. The optical mounting is illustrated in Figure 1b. For this purpose, the laser was focused on the backside of the sample and the signal was collected on the top surface of the sample. The intensity of transmission was evaluated by subtracting the baseline (black body radiation) and by integrating both the intensity of transmitted excitation of laser and Rayleigh scattering intensity (unresolved by our equipment's). Assuming the Beer-Lambert absorption in function of the penetration depth z, the transmitted intensity is given by:

$$I(z,T)/I(0,T) = e^{-\alpha(\lambda_{LASER},T)z} \quad (2)$$

Where $I(0,T)$ is the incident laser intensity at wavelength λ_{LASER}, and $\alpha(\lambda_{LASER},T)$ is the coefficient of absorption. The subsequent changes of transmission with temperature may occur due to phase transition, changes in microstructure or variations in photon absorption. No intensity variations were observed after several thermal cycles and we can assume that no significant changes of microstructure occurred during the time of our experiment (limited to a few minutes at 1500 °C). From Equation 2, the changes of absorption coefficient at the laser wavelength and for fixed thickness of sample, (d is almost the same for all our samples ~200 µm) was measured as a function of temperature. The absorption at different temperatures and for the different samples was normalized with respect to the absorption at RT (about 24 °C (± 1 °C) given by $\frac{\alpha(\omega_{LASER},T)}{\alpha(\omega_{LASER},RT)}$.

3. Results

The Raman spectra of m-ZrO_2, TBC, YSZ(111) and 38%YSZ samples (described in Table I), measured at RT using the same experimental conditions (objective lens, laser intensity, counting time) using 355 nm and 532 nm excitation are presented in Figure 2. The Raman intensity depends on the incident and scattered polarization [perry1980], [fukatsu2010]. To decrease the dependence on the orientation, unpolarized spectra of several orientations were averaged in our experiments as described in [perry1980]. The analysis of the modes at low frequencies are limited to 150–200 cm^{-1} due to cut by the UV notch and so no information on the Rayleigh scattering and central peak can be obtained. The Stokes first-order Raman spectra are within 50 cm^{-1} to 800 cm^{-1}. The increase of the symmetry from monoclinic, tetragonal to cubic phases is observed by a decrease in the number of modes and an increase in their damping. A decrease of mode intensity with wavenumber of around 600 cm^{-1} by increasing the yttria content from monoclinic to cubic phases was observed in agreement with previous studies [liu1988],[cai1995]. This mode corresponds to Raman active F_{2g} mode in the cubic phase [feinberg1980], [perry1990], [cai1995]. Other bands of c-ZrO_2 correspond to disorder induced scattering out of the centre of the Brillouin zone. In particular, the modes below 400 cm^{-1} in c-ZrO_2 are related to acoustic density of state. The intensities of cubic specimens (YSZ111 and

38%YSZ) were considerably lower than those of m-ZrO_2 and t'-YSZ. The integrated UV Raman intensity from 150 to 850 cm^{-1} of the different samples shows that the area normalized with respect to that m-ZrO_2 was about 3.7 times for TBC, 1.5 for YSZ(111) and 0.8 for 38%YSZ. The relative intensities measured using 532 nm laser excitation were 3 for TBC and 0.5 for both cubic samples. In the case of 355 nm excitation, little difference in the Raman spectra of cubic YSZ(111) and 38%YSZ samples are due to the composition factor whereas the Raman modes of 38%YSZ presented higher damping (width) than YSZ(111) due to higher with Y_2O_3 concentration.

The UV Raman spectra of m-ZrO_2, TBC, YSZ(111) and 38%YSZ samples as a function of temperature are presented in Supplementary Material. It is important to note that no phase change or decomposition due to temperature cycles were observed for all studied samples. The intensity variations of each mode in the spectra are out of the scope of this paper. Indeed, the analysis of Raman modes at high temperature (frequencies shift, broadening) cannot be fitted by simple profiles. Thus, instead of studying the Raman intensities of individual modes, the integrated intensity of the first order Raman spectra (integrated intensity from the notch cut at 150 cm^{-1} to 850 cm^{-1}) as a function of temperature is presented in Figure 3 using relative scale, normalized with respect to the Raman intensity of m-ZrO_2 (given in Figure 2). It is important to note that the integrated Raman intensities, presented in Figure 3, were obtained after the subtraction of thermal emission registered during the experiment but without laser excitation. A residual background was still present in m-ZrO_2 after subtraction due to photoluminescence (F-centre) and was corrected by a linear baseline in the wavenumber range of Raman spectra. The temperature dependence of Raman spectra is additionally compared to the contribution of Bose-Einstein factor, of Equation 1, $1 + n(\omega_{phonon})$, representing the phonon population calculated for a phonon energy of ω_{phonon} =0.07 eV (600 cm^{-1}). This factor increases as a function of temperature by a factor of 2.5 when temperature is increased from RT to 1500 °C. The Raman intensity of c-ZrO_2 samples increases from RT to 800° slightly faster when predicted by the Bose-Einstein factor, it presents maximum intensity at around 800 °C and it decays by about one order of magnitude with further increase of the temperature up to 1500 °C. In the case of TBC, the Raman intensity remains constant, independent of the Bose-Einstein factor, up to around 700 °C. Its Raman intensity decreases slowly from 800 °C to 1100 °C, and, then decrease above 1200 °C similarly to that of the cubic YSZ samples. It is important to note that the changes of Raman intensity as a function of temperature of m-ZrO_2 is very different from the other studied specimens. Raman intensity of m-ZrO_2 presents a maximum of intensity at around 400 °C. From 400 °C up to 1200 °C, the Raman intensity of zirconia decreases slowly (quite independent of Bose-Einstein factor). At 1200 °C, the Raman intensity at the phase transition from monoclinic to tetragonal phase drops from 5 to 10% followed by a continuous slow decrease with further increase in the temperature. At the phase transition, the Raman intensity between monoclinic and tetragonal phases is similar and does not show anomalies like the Raman intensity of the t' phase at room temperature (3.7 times stronger than that of the monoclinic phase).

To further investigate the thermal emission, the integrated intensity above the first-order Raman modes is presented in Figure 4. The integrated intensities registered around 367 nm +/-0.5 nm

(Raman shift of about 1000 cm^{-1} with the laser excitation 355 nm). In addition, Figure 4 presents the intensity of thermal emission measured experimentally without laser excitation and the intensity of the Planck-black body radiation near the excitation wavelength (ω_{photon}=367 nm), by evaluating the Bose-Einstein factor, $n(\omega_{photon})$, as a function of temperature. All the data is normalized to 1 at 1500 °C, which correspond to state at which the thermal emissivity is dominant. In Figure 4, the intensity of a black body radiation increases with the increase in temperature. Some differences in thermal emission are observed between the different samples without laser excitation. An excellent matching is found between Planck blackbody radiation and experimental data without laser excitation at high temperature (Figure 4). A good matching is also found on the integrated intensities at 367 nm of m-ZrO_2, TBC, YSZ(111) and 38%YSZ samples with 355 nm laser excitation above 1200 °C. Meanwhile, the temperature variation of intensity shows significant difference below 1000 °C. The 367 nm wavelength has been chosen as it is above first order Raman spectra. In the case of m-ZrO_2 sample, a fluorescence contribution at low temperature will be later investigated. For TBC, YSZ(111) and 38%YSZ samples, the residual intensity observed can be related to the second order Raman scattering. These background contributions present a higher amplitude for TBC than c-ZrO_2 samples and a maximum around 1000–1100°C, before, the black body thermal radiation dominated the emission intensity.

To understand the decrease of Raman intensity at high temperature, the absorption of the laser has been evaluated by transmission measurements of the different thinned samples of m-ZrO_2, TBC, YSZ(111) and 38%YSZ (Figure 5) as described in experimental details section. The decrease of transmission intensities was significant in the 1200–1500 °C temperature range with respect to the transmission at room temperature. However, the evolution trends depend on the amount of yttria in the sample. The cubic zirconia, YSZ(111) and 38%YSZ specimens, presented an increase of transmission up to 700–900 °C, followed by a drop by several orders of magnitude. The UV transmission of TBC presented no clear maxima and started to decay at 400–500 °C, the behaviour was similar in the case of cubic samples above 900 °C. Finally, the UV transmission of m-ZrO_2 gradually decreased from room temperature to 1500 °C. It presented a small increase in intensity at the monoclinic-tetragonal phase transition (around 1200 °C) and it decreased above the transition. A set of measurements was done to scan the change of UV transmission during the monoclinic-tetragonal phase transition during heating and cooling cycles (presented in Figure 7). The anomalous transmission peak observed at phase transition shows a hysteresis during heating and cooling cycles with maxima at 1200 °C and 1050 °C, respectively. Similar hysteresis has been observed in ZrO_2 and HfO_2 by Raman scattering [perry1980], [fujimori2001] and it was not investigated further in this paper. The maximum transmission shifted towards the high temperature side with the increase of the yttria concentration, also, the transmission dropped by 3 to 4 orders of magnitude from RT to 1500 °C, whereas the Raman scattering dropped only by one order of magnitude.

The temperature dependence of UV transmission (Figure 5) has been fitted by using a model of a single thermally activated decay [petrik1999]:

$$I(T) = \frac{I_0}{1+Ae^{E_A/kT}} \quad (3)$$

Where E_A is the activation energy of the thermal quenching process, k – the Boltzmann constant, T – temperature, I_0 – the integrated intensity at room temperature, and A – a constant. It was found that the activation energy was 2.7 eV for TBC and 2.9 eV for YSZ(111) and 38%YSZ. In the case of 38%YSZ, an additional deviation in temperature dependence of UV transmittance with corresponding activation energy of around 4–5 eV appeared above 1400 °C. However, m-ZrO_2 presented a singular thermal quenching process without activation energy contrary to the processes observed in alloyed samples. It is to be noted that contrary to other samples the transmission of m-ZrO_2 increases from room temperature to about 300 °C. Complementary photoluminescence and Raman scattering measurements from RT to 900 °C (with temperature increasing steps of 25 °C) are presented in Supplementary Material (Figure A3).

4. Discussion

Electronic structure of YSZ has been subjected to numerous studies at room temperature, but its role at high temperature has received little attention. An increase of absorption by 3–4 orders of magnitude at the ultraviolet laser frequency was observed with the increase of temperature in all our samples meanwhile Raman scattering at high temperature remained strong. The first order Raman scattering intensity is described by Equation 1 (commonly used to analyse transparent dielectric materials in the proximity of room temperature (up to 300 °C), but this Equation is not valid under ultraviolet excitation and at high temperature. These results indicate that resonant scattering should compensate the laser absorption.

Loudon's theory of Resonant Raman scattering intensity

The Raman scattering spectra does not vanish at high temperature when laser absorption increase. This result suggests that an electronic resonance occurs. To further analyse high-temperature Raman intensity, we will refer to Loudon theory of resonance Raman scattering [loudon1965]. The connection of incident absorption, $\alpha(\omega_{LASER}, T)$, and gain of resonant Raman scattering, $R(\omega_{ph})$, is given by:

$$I_{Raman}(T)/I_{LASER} = R(\omega_{ph})(1 - e^{-2\alpha(\omega_{LASER},T)l})/(2\alpha(\omega_{LASER}, T)) \quad (4)$$

with $2l$ – the scattering penetration length in forward and backward light scattering. In Equation 4, we assume that R<<$\alpha(\omega_{LASER}, T) \approx \alpha(\omega_{Raman}, T)$ of Loudon's theory. In the case of weak absorption ($\alpha(\omega_{LASER}, T) \sim 0$), this Equation tends to $I_{Raman}(T)/I_{LASER} = R(\omega_{ph})l$ i.e. Raman intensity is proportional to the scattering volume as in Equation 1. However, in the case of resonant strong absorption, $I_{Raman}(T)/I_{LASER} = R(\omega_{ph})/(2\alpha(\omega_{LASER}, T))$. This result clearly shows that single Beer-Lambert exponential decay factor $e^{-2\alpha(\omega_{LASER},T)l}$ vanish at resonance. The Raman intensity varies inversely with the coefficient of absorption.

In the Figure 6, we analyse the high temperature Raman spectra in the different samples by plotting Equation 4 and using the Equation 2 where $e^{-2\alpha(\omega_{LASER},T)l} = [I(z,T)/I(0,T)]^2$ and Equation 3 with $\alpha(\omega_{LASER}, T) = log\frac{I(d,T)}{I(0,T)}$. It worth noting that, the term 1/ $log\frac{I(d,T)}{I(0,T)}$ diverges

because of the normalization of the transmission $\frac{I(d,T)}{I(0,T)}$ at room temperature. However, the numerator converges to zero. So, the ratio of $I_{Raman}(RT)/I_{LASER}$ is finite. It has been normalized to 1 in Figure 6 at room temperature. In addition, we add in Equation 4 the Bose-Einstein factor of Equation 1 to include the temperature factor given by first order Raman scattering. In the following section, different samples will be compared.

Monoclinic zirconia

Pure monoclinic zirconia (m-ZrO_2) presented strong F-centre photoluminescence near room temperature (as seen in the background in Figure 3 and in Figure A3). The intensity of photoluminescence quenched rapidly around 300–400 °C. F-centre absorption induced a drop of intensity by 40%. The Raman scattering intensity at room temperature was then corrected by a same factor. We can note that there is no Raman resonance effect due to F-centre energy level near room temperature. However, at high temperature, the drops of laser transmission and the slow decrease of Raman scattering, is fully compatible with a Raman resonance effect with absorption data. Meanwhile, the Raman intensity indicates more probably a pre-resonance effect, i.e. no crossover energy is observed. As for the change of transmission at the phase transition appearing at the martensitic phase transition of Figure 7. The increase of absorption is possibly related to the nucleation of second-order phase transition or to some renormalization of energy levels which induce accidentally higher absorption at our excitation wavelength. One can note that anomalous enhanced Raman scattering as also been controversial in quartz and related to α→β domain [shapiro1968]. Finally, we can note that the amplitude of Raman susceptibility of the high temperature tetragonal phase is similar (within 5–10%) to the monoclinic phase near the phase transition. This result confirms that Raman scattering efficiency of monoclinic and tetragonal phase are of the same magnitude [feinberg1980], [perry1990], [cai1995], but contradicted the room temperature high Raman scattering efficiency observed in t' zirconia, as discussed below.

t' zirconia

A first observation concerns the strong Raman intensity of TBC sample below 1000 °C (Figures 2 and 3). The Raman intensity of t' is 3 to 4 times stronger than the integrated intensity of monoclinic or cubic zirconia with 532 nm or 355 nm laser excitation. (This observation also remains valid after absorption correction of F-centre in the monoclinic sample in the UV.) As this phenomenon is independent of the laser energy and temperature up to 1000 °C, the strong intensity of TBC is not expected to be related to an electronic resonance. The Raman intensity of the stable tetragonal phase (t-YSZ) with dopant stabilization was not reported to be specifically anomalous in the literature [feinberg1980], [perry1990], [cai1995].

As all Raman spectra were obtained within the same experimental conditions (Figure 2), one should argue that the difference in Raman intensity of the t' sample could be due to its columnar microstructure of the TBC. Guided light and multi-scattered phenomena through the columnar grain could increase the back and forward light penetration length. However, the optical scattering of light usually decreases the scattered intensity due to void or birefringence [limarga2009], [klimke2011]. This potential origin of an increased intensity of TBC was

checked by measuring the Raman spectra of TBC powder (fabricated by crushing textured TBC) and of a cross section of columnar TBC. The observed intensities of all different TBC specimens were considerably higher than that of monoclinic or cubic zirconia.

The coherent twinned domain pattern [ishizawa1986] could be suspected of being responsible. This hypothesis is investigated in the following, considering that the anomalous high intensity of TBC observed at room temperature and at different excitation wavelength is not due to a resonant Raman susceptibility $R(\omega_{ph})$ of t'-YSZ. Indeed, a relation has been established by Maradudin and Burstein to evaluate the Raman polarizability in relation to photoelasticity and electrostriction (Equation 5.19 in [maradudin1967]). The microscopic model, established for cubic diamond structure, shows that the Raman polarizability increases as the square of lattice dielectric constant ε_0^2 and depends on the photoelastic anisotropy. In our case, the integrated Raman intensity, increased in the sequence I(m-ZrO_2)<I(cubic) <I(t'-TBC) following the same sequence as the static dielectric constant calculated ε_0 (monoclinic)~16 < ε_0 (cubic)=32 < ε_0 (tetragonal) ~42 [rignanese2001],[zhao2002],[fadda2010]. Also, the dependence on photoelastic anisotropy follows the measurements of Chistyi et al. [chistyi1977]. They observed an increase of photoelastic coefficients approaching the tetragonal phase by decreasing Y_2O_3 content in cubic YSZ. The existence of nonlinear terms in photoelasticity and electrostriction are due to the ferroelastic t' zirconia due to internal strains in the twinned domain structure [ishizawa1986]. Indeed, the extreme high toughness of tetragonal zirconia has already been attributed to the ferroelastic phase. Moreover, the ability to transform deformation (phonon) under light excitation by photoelasticity may also be contributed to the decay of phonons mean free path and explain the low thermal conductivity of TBC [yashima1996], [mévrel2004], [chevalier2009]. In conclusion, enhanced Raman susceptibility of TBC sample at room temperature are intimately related to the ferroelastic t'-ZrO_2 phase and far from resonance. Indeed, the temperature Raman scattering efficiency of t' show a resonance above 1000 °C that is well described by the resonance effect of Equation 4. Additionally, the Raman and transmission data were similar after several cycles of experiment and the room temperature spectra of TBC were identical, and so no degradation was observed within our experimental uncertainty. The intensity of Raman resonance is the dominant effect observed at high temperature and it is very well explained with an energy level absorption cross over with our laser excitation.

Cubic zirconia

In the case of cubic, no structural change occurs in the studied range of temperature, thus, the Raman polarizability shouldn't change abruptly. The minor deviation of Raman intensity from the Bose-Einstein factor below 1000 °C indicates that higher order Raman scattering terms in $n(\omega_{ph}, T)^2$ or pre-resonance intensity should also contribute. The second order scattering is, however, no more observable above this temperature due to the dominant thermal black body radiation. The increase of absorption with resonance Raman scattering appears at high temperature. However, one can note that the resonance maxima obtained from the UV transmission of Equation 4, and the Raman intensities are shifted in temperature by 200–300 °C. Also, above 1200 °C, the decrease of Raman scattering is slower than the one calculated

from the absorption data of Equation 4. We suspect that the absorption is composed of resonant energy levels and some other defects that do not induce resonance but absorb some of the intensity.

Conclusion

Ultraviolet Raman scattering and transmission of undoped and yttria doped ZrO_2 with different structures has been studied in the temperature range from room temperature to 1500 °C. Temperature Raman spectra below 1000 °C deviate from first order Raman scattering intensity, described by Equation 1. Resonant Raman scattering is involved at 355 nm excitation. The increase of absorption above 800 °C is clearly associated with the band gap energy crossover the laser excitation. Loudon's theory of Raman resonance intensity in Equation 4 described quantitatively the resonances observed experimentally. Meanwhile, one can note that the changes in absorption and Raman intensity are slightly shifted in temperature due to the absorption by other defects below the band gap. These defects play an important role in the transport properties of YSZ and could be finely studied by the proposed method. Our data additionally suggest that the strong Raman intensity of t'-YSZ of TBC at room temperature should be attributed to the ferroelastic domains of this metastable phase and not to the resonance effect. A systematic study of Raman scattering intensity of t' phase as function of yttria composition or aging could be used to measure quantitatively the properties of TBC. In comparison, the Raman scattering intensity of the high-temperature tetragonal phase of ZrO_2 does not show an enhanced intensity as t' phase indicating a difference in its properties.

Acknowledgements

This work has received the financial support of ONERA-The French Aerospace Lab, in the framework of the French Carnot project CENDRE, Bourgogne Franche-Comté region, and EUR EIPHI program grant number ANR-17-EURE-0002, French RENATECH network and its FEMTO-ST technological facility. The authors thank Marie-Hélène Vidal-Sétif, Catherine Rio and Odile Lavigne (ONERA) for supplying the samples and helpful comments on the manuscript. Solène Ropers is also greatly acknowledged for her technical assistance.

References

[miller1997] R.A. Miller, *J. Thermal Spray Technol.* **1997**, 6, 35, DOI: 10.1007/BF02646310

[ikeda1985] S. Ikeda, O. Sakurai, K. Uematsu, N. Mizutani, M. Kato, *J. Mat. Sci.* **1985**, 20, 4593, DOI: 10.1007/BF00559349

[Vladislav1999] V.V. Kharton, E.N. Naumovich, A.A. Vecher, *J. Solid State Electrochem.* **1999**, 3, 61, DOI: 10.1007/s100080050

[scott1975] H.G. Scott, *J. Mat. Sci.* **1975**, 10, 1527, DOI: 10.1007/BF01031853

[garvie1975] R. C. Garvie, R.H. Hannink, R.T. Pascoe, *Nature* **1975**, 258(5537), 703–704. doi:10.1038/258703a0

[Heimann2015] Robert B. Heimann, Hans D. Lehmann, Bioceramic Coatings for Medical Implants, **2015**, Wiley-VCH Verlag GmbH & Co. KGaA, ISBN:9783527337439

[chevalier2009] J. Chevalier, L. Gremillard, A.V. Virkar, D.R. Clarke, *J. Am. Ceram. Soc.* **2009**, 92 (9), 1901, DOI: 10.1111/j.1551-2916.2009.03278.x

[evans2008] A.G. Evans , D.R. Clarke, C.G. Levi, *J. Eur. Ceram. Soc.* **2008**, 28 (7), 1405, DOI: 10.1016/j.jeurceramsoc.2007.12.023

[Morelli2020] S. Morelli, V. Testa, G. Bolelli, O. Ligabue, E. Molinari, N. Antolotti, L. Lusvarghi, *Journal of the European Ceramic Society* **2020**, 40(12), 4084–4100, DOI: 10.1016/j.jeurceramsoc.2020.04.058

[zhu2020] W. Zhu, S. Nakashima, E. Marin, H. Gu, G. Pezzotti, *J Mater Sci* **2020**, 55, 524–534 DOI: 10.1007/s10853-019-04080-9

[cai2020] H. Cai, X. Zhang, L. Hu, F. Guo, X. Wang, X. Zhao, N. Ni, P. Xiao, *Int J Appl Ceram Technol.* **2020,** 17[5], 2416–2423, DOI: 10.1111/ijac.13542

[mevrel2004] R. Mévrel, J.-C. Laizet, A. Azzopardi, B. Leclercq, M. Poulain, O. Lavigne, D. Demange, *J. Eur. Ceram. Soc.* **2004**, 24, 3081, DOI: 10.1016/j.jeurceramsoc.2003.10.045

[Ngai2013] K.L. Ngai, J. Santamaria, C. Leon, *Eur. Phys. J. B*, **2013**, 86, 7, DOI: 10.1140/epjb/e2012-30737-2

[ishizawa1986] N. Ishizawa, A Saiki, T Yagi, N. Mizutani, M. Kato, *J. Am. Ceram.* Soc. **1986**, 69(2), C-18, DOI: 10.1111/j.1151-2916.1986.tb04724.x

[ishigame1977] M. Ishigame, T. Sakurai, *J. Am. Ceram. Soc.* **1977**, 60 (7-8), 367 DOI: 10.1111/j.1151-2916.1977.tb15561.x

[Clarke1982] D.R Clarke, & F. Adar, *J. Am. Ceram. Soc.* 1982, 65(6), 284–288. j.1151-2916.1982.tb10445.x

[perry1990] C. H. Perry, F. Lu, D. W. Liu, B. Alzyab, J. Raman Spec. **1990**, 21, 577, DOI: 10.1002/jrs.1250210909

[feinberg1981] A. Feinberg, C.H. Perry, *J. Phys. Chem. Solids* **1981**, 42 (6), 513, DOI: 10.1016/0022-3697(81)90032-9

[cai1995] J. Cai, C. Raptis, Y. S. Raptis, E. Anastassakis, *Phys. Rev. B* **1995**, 51, 201 (1995), DOI: 10.1103/PhysRevB.51.201

[margueron2014] S. Margueron, D.R. Clarke, *J. of Appl. Physics* **2014**, 116(19):193101, DOI: 10.1063/1.4901833

[lughi2007] V. Lughi, D.R. Clarke, *J. Appl. Phys.* **2007**, 101, 053524 DOI: 10.1063/1.2697347

[lughi2005] V. Lughi, , D.R. Clarke *J. Am. Ceram. Soc.* **2005**, 88(9), 2552–2558. 10.1111/j.1551-2916.2005.00452.x

[gouadec2007] G. Gouadec, Ph. Colomban, *Progr. Crystal Growth Charact. Mater.* **2007**, 53 (1), 1, DOI: 10.1016/j.pcrysgrow.2007.01.001

[fukatsu2010] K. Fukatsu, W. Zhu, G. Pezzotti, *Phys. Status Solidi B* **2010**, 247 (2), 278, DOI: 10.1002/pssb.200945358

[liu1988] D.W. Liu, C.H. Perry, R.P. Ingel, *J. Appl. Phys.* **1988**, 64, 1413, DOI: 10.1063/1.341839

[Salnikov2000] V. V. Sal'nikov, *Inorg. Mater.* **2000**, 36 (5), 479, DOI: 10.1007/BF02758052

[macrae2008] C.M. MacRae, N.C. Wilson, *Microsc. Microanal.* **2008**, 14, 184, DOI: 10.1017/S143192760808029X

[hachiya2005] K. Hachiya, H. Oku, *Phys. Rev. B* **2005**, 71, 064111, DOI: 10.1103/PhysRevB.71.064111

[cui2015] J. Cui, G. A. Hope, *Journal of Spectroscopy* **2015**, Article ID 940172, DOI: 10.1155/2015/940172

[fujimori2001] H. Fujimori, M. Yashima, M. Kakihana, M. Yoshimura, *J. Am. Ceram. Soc.* **2001**, 84 (3), 663, DOI: 10.1111/j.1151-2916.2001.tb00721.x

[petrik1999] N.G. Petrik, D.P. Taylor, T.M. Orlando, *J. Appl. Phys.* **1999**, 85, 6770 DOI: 10.1063/1.370192

[loudon1965] R. Loudon, *J. Phys. France* **1965**, 26(11), 667 DOI: 10.1051/jphys:019650026011067700

[wiemhofer1992] H.-D. Wiemhofer, U. Vohrer, *Ber. Bunsenges. Phys. Chem.* **1992**, 96(11), 1646, DOI: 10.1002/bbpc.19920961123

[Sanchez2006] J. Sanchez-Gonzalez, A. Dıaz-Parralejo, A.L. Ortiz, F. Guiberteau, *Appl. Surface Sci.* **2006**, 252, 6013, DOI: 10.1016/j.apsusc.2005.11.009

[heiroth2011] S. Heiroth, R. Ghisleni, T. Lippert, J. Michler, A. Wokaun, *Acta Materialia* **2011**, 59, 2330–2340, DOI: 10.1016/j.actamat.2010.12.029

[morell1997] G. Morell, R.S. Katiyar, D. Torres, S.E. Paje, J. Llopis, *J. Appl. Phys.* **1997**, 81, 2830 DOI: 10.1063/1.363941

[french1994] R. H. French, S. J. Glass, F. S. Ohuchi, Y. -N. Xu, W. Y. Ching, Phys. Rev. B 1994, 49(8), 5133, DOI: 10.1103/PhysRevB.49.5133

[rignanese2001] G.-M. Rignanese, F. Detraux, X. Gonze, A. Pasquarello, *Phys. Rev. B* **2001**, 64, 134301, DOI: 10.1103/PhysRevB.64.134301

[zhao2002] X. Zhao, D. Vanderbilt, *Phys. Rev. B* **2002**, 65, 075105, DOI: 10.1103/PhysRevB.65.075105

[garcia2006] J. C. Garcia, L. M. R. Scolfaro, A. T. Lino, V. N. Freire, G. A. Farias, C. C. Silva, H. W. Leite Alves, S. C. P. Rodrigues, E. F. da Silva, *J. Appl. Phys.* **2006**, 100, 104103, DOI: 10.1063/1.2386967

[fadda2010] G. Fadda, G. Zanzotto, L. Colombo, *Phys. Rev. B* **2010**, 82, 064106, DOI: 10.1103/PhysRevB.82.064106

[liu2011] Q.-J. Liu, Z.-T. Liu, L.-P. Feng, *Physica B* **2011**, 406, 345, DOI: 10.1016/j.physb.2010.10.057

[youssef2012] M. Youssef, B. Yildiz, *Phys. Rev. B* **2012**, 86, 144109, DOI: 10.1103/PhysRevB.86.144109

[camagni1992] P. Camagni, P. Galinetto, G. Samoggia, N. Zema, *Solid State Comm.* **1992**, 83(11), 943 DOI: 10.1016/0038-1098(92)90916-W

[llopis1990] J. Llopis, *phys. stat. sol. (a)* **1990**, 119, 661, DOI: 10.1002/pssa.2211190230

[limarga2009] A.M. Limarga, D.R. Clarke, *Int. J. Appl. Ceram. Technol.* **2009**, 6 (3), 400, DOI: 10.1111/j.1744-7402.2008.02349.x

[klimke2011] J. Klimke, M. Trunec A. Krell, *J. Am. Ceram. Soc.* **2011**, 94 (6) 1850, DOI: 10.1111/j.1551-2916.2010.04322.x

[maradudin1967] A.A. Maradudin, E. Burstein, *Phys. Rev.* **1967**, 164 (3), 1081, DOI: 10.1103/PhysRev.164.1081

[Chistyi1977] I. L. Chistyi, I. L. Fabelinskii, V. F. Kitaeva, V. V. Osiko, Y. U. V. Pisarevskii, I. M. Sil'Vestrova, N. N. Sobolev, *Journal of Raman spectroscopy* **1977**, 6(4), 183, DOI: 10.1002/jrs.1250060406

[shapiro1968] S. M. Shapiro, H. Z. Cummins, *Phys. Rev. Lett.* **1968**, 21, 1578, DOI: 10.1103/PhysRevLett.21.1578

Table I Structure and composition of studied doped and undoped zirconia specimens.

Sample name	Structure at RT	Remarks	Composition in wt% (± 1 %)		
			ZrO_2	HfO_2[a]	Y_2O_3
m-ZrO_2	Monoclinic zirconia	Twinned single crystal	98.0	2.0	0
TBC or t'-YSZ	t'-yttria partially stabilized zirconia[b]	Spall of TBC 125 µm thick, columnar microstructure	89.3	1.9	8.8
YSZ(111)	Cubic yttria stabilized zirconia	(111) oriented crystal wafer	78.5	2.1	19.4
38%YSZ	Cubic yttria stabilized zirconia	Unoriented single crystal	60.4	1.4	38.3

[a] Hafnia is a natural impurity in zirconia systems.

[b] t' – metastable tetragonal phase

FIGURES

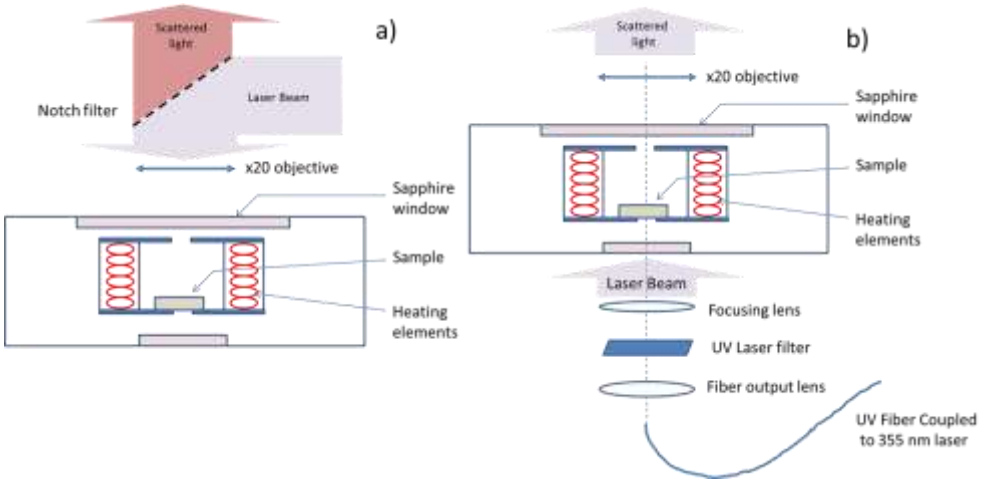

FIGURE 1 Experimental setup used for measurements of Raman and ultraviolet transmission measurement as a function of temperature.

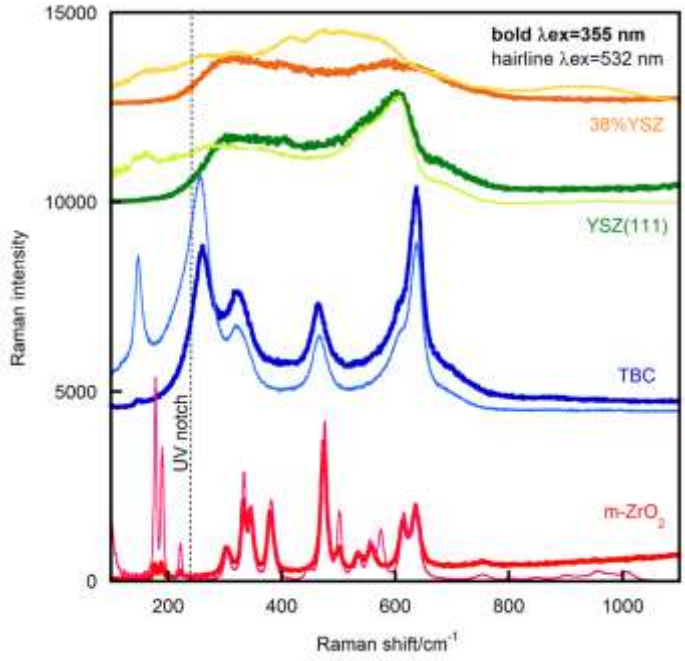

FIGURE 2 Raman spectra at room temperature and measured in the same conditions of m-ZrO_2, TBC, YSZ(111) and 38%YSZ using 355 nm and 532 nm laser excitation.

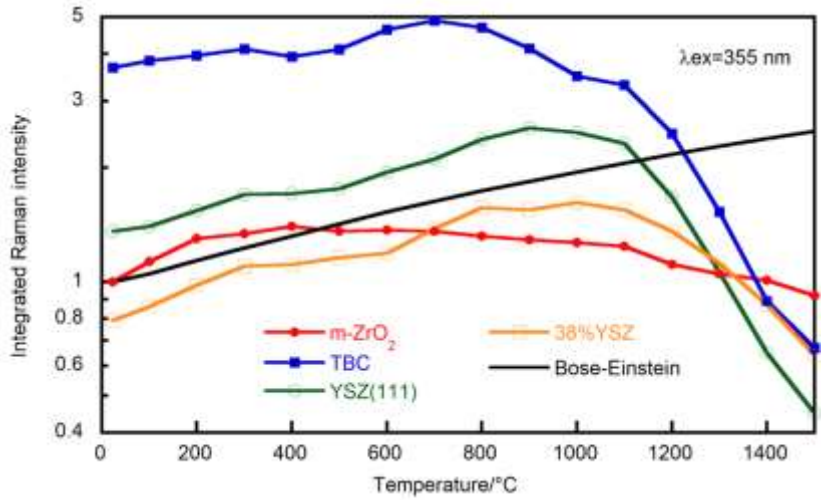

FIGURE 3 Integrated Raman intensity in the spectral range from 150 cm^{-1} to 850 cm^{-1} as a function of the temperature for m-ZrO_2, TBC, YSZ(111) and 38%YSZ, and plot of Bose-Einstein factor.

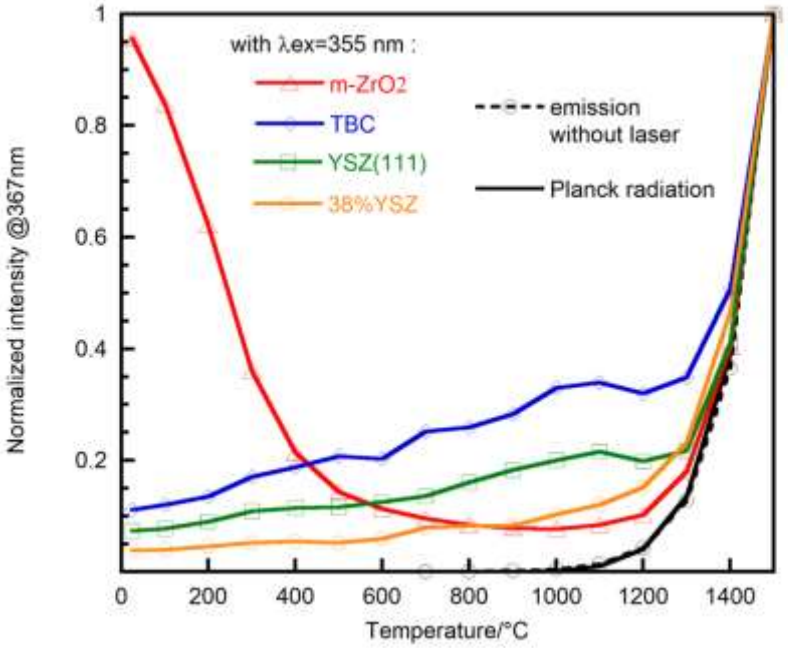

FIGURE 4 Intensity of thermal emission as a function of temperature, measured at 367 nm with and without laser excitation on m-ZrO_2, TBC, YSZ(111) and 38%YSZ specimens, in comparison to the calculated Planck's black body radiation at a wavelength of 367 nm.

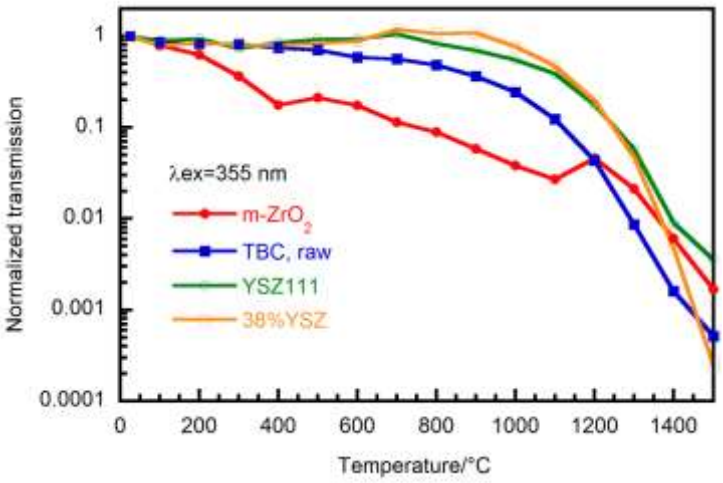

FIGURE 5 Temperature dependence of 355 nm-laser transmission for m-ZrO_2, TBC, YSZ(111) and 38%YSZ samples (intensity represented in logarithmic scale).

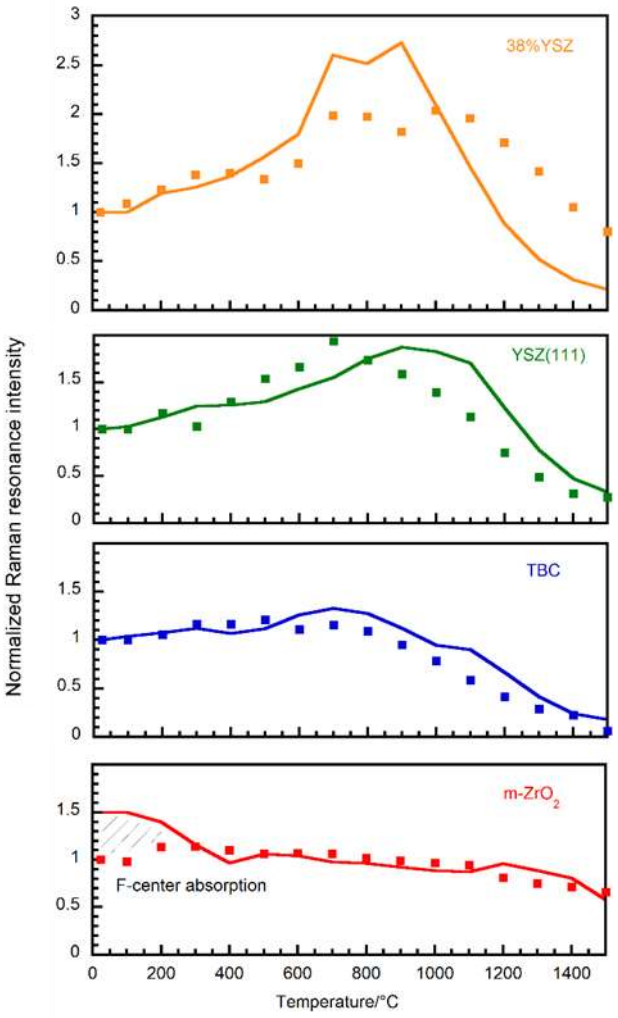

FIGURE 6 Resonant Raman scattering intensity calculated using Loudon's model of Equation 4 (line) and experimental data of Figure 5 (dots).

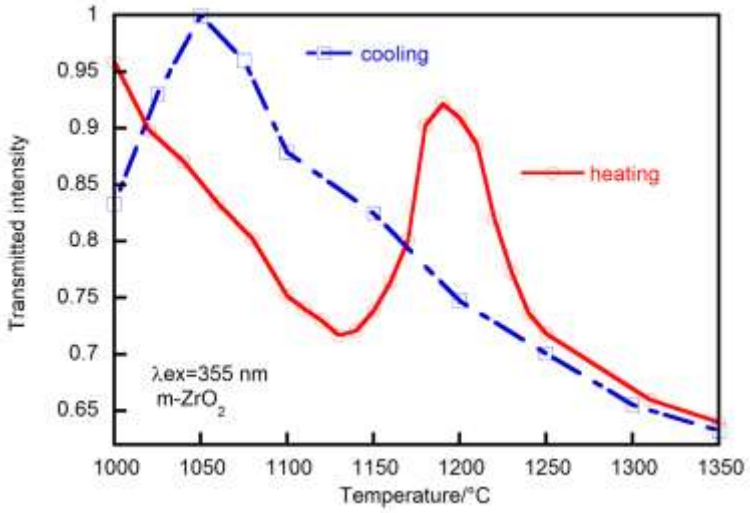

FIGURE 7 UV-laser transmission during the monoclinic to tetragonal phase transition observed during heating and cooling (5 °C/min) cycles.

SUPPLEMENTARY MATERIAL

Luminescence and impurities in YSZ samples

We have additionally investigated the photoluminescence spectra of m-ZrO_2, TBC, YSZ(111) and 38%YSZ samples, excited at 355 nm and 266 nm at room temperature (Figure A1). The photoluminescence showed a strong dependence on the sample structure and excitation wavelength. The emission intensities are given in the same experimental conditions, but the spectrometer response is not calibrated. The monoclinic m-ZrO_2 sample presents a strong emission centred around 480 nm (two orders of magnitude stronger than other samples) at 355 nm and 266 nm excitations. Additionally, the photoluminescence band presented a long lifetime and phosphorescent in dark after UV irradiation. This emission band has been intensively studied by cathodoluminescence and has been attributed to F-centres induced by interstitial oxygen defects [Sal'nikov2000, MacRae2008]. The emission excited at 266 nm is a slightly broader than that excited at 355 nm, with an additional emission induced around 560 nm. The temperature emission of this band will be more deeply investigated in Figure A3 and A4. The t'-ZrO_2 and c-ZrO_2 samples present fine emission lines excited at 355 nm and several broad photoluminescence bands at 266 nm with considerably less pronounced intensity than those of monoclinic sample. The emission of TBC excited at 266 nm has a band centred around 560–580 nm, like the one observed by Hachiya [Hachiya2005]. The emission of c-ZrO_2 monocristal, excited at 266 nm, present a band centred around 580–590 nm. The energy of this band is similar to that of monoclinic zirconia but with two orders of magnitude less intensity and an asymmetric tail in red shift that can be superposed to the one of TBC.

As for the emission of TBC excited at 355 nm, it presents no broad emission, but chromium emission line from Cr^{3+}:Al_2O_3 at 693 nm from thermally grown alumina that remained attached to the TBC. It also presents emission lines at 480 nm, 580 nm and 675 nm that can be attributed to $^4F_{9/2}$ to $^6H_{15/2}$, $^6H_{13/2}$ and $^6H_{11/2}$ transitions respectively of dysprosium rare earth impurities. Similar impurities lines are observed in 38%YSZ and are also attributed to dysprosium, while, YSZ(111) presents impurity lines associated with Gd_2O_3 luminescence [cui2015]. One can note that the emission of impurities is much smaller with 266 nm excitation. Broad emission spectra of zirconia are dominating and are not affected by the presence of the different impurities. The 266 nm laser line is likely above the band gap, and little energy transfer is observed to the impurities. From these measurements, it seems that the defect luminescence span in the entire visible frequency range with two bands at ~480 nm and ~560 nm which can appear in all yttria compositions and crystallographic structures.

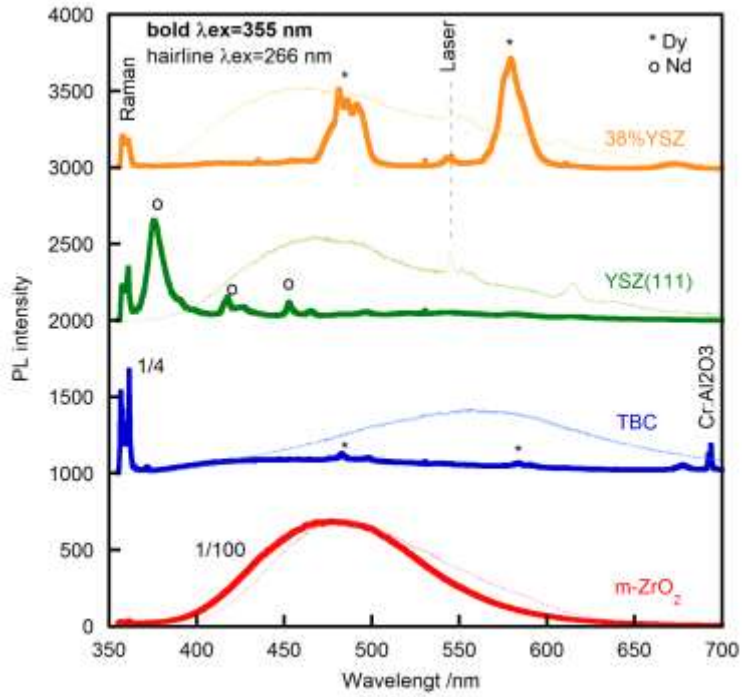

FIGURE A1 Photoluminescence spectra of m-ZrO_2, TBC, YSZ(111) and 38%YSZ measured by using 355 nm and 266 nm laser excitation at RT. The multiplication factors of m-ZrO_2 and TBC are indicated to fit the figure. Some impurities and 2nd order line of 266 nm are marked.

Electronic levels in YSZ and transmission

The band structure of monoclinic ZrO_2, tetragonal and cubic YSZ present a band gap between 5.2 eV to 4 eV respectively [wiemhofer1992], [Sanchez2006], [heiroth2011]. *Ab initio* calculations had determined that the band gap is indirect [french1994], [rignanese2001], [zhao2002], [garcia2006], [fadda2010], [liu2011]. The laser excitation (355 nm / 3.49 eV) at room temperature is below the gap absorption and show the first order Raman scattering at room temperature. However, the temperature red shift of the band gap is approximately -0.3 meV/K [wiemhofer1992]. Thus, the band gap should decrease by -0.5 eV at 1500 °C and therefore it should approach our laser energy in the case of tetragonal and cubic structures.

Luminescence emission under 266 nm excitation at room temperature is presented in Figure A1. The emission may correspond to intrinsic defect recombination centre and mid-gap recombination from photo-excited electrons. The exact position of this level is difficult to evaluate due to the strong Stoke shift by lattice relaxation of excited levels. It is obvious, in the case of m-ZrO_2, that the strong fluorescence centred at 480 nm (2.6 eV) is an electron trap in a vacancy (F-centre). The absorption of this level is close to the laser excitation at room temperature (355 nm/3.49 eV) and relaxed by 1 eV. The luminescence is rapidly quenched in temperature, suggesting that the electrons are no more trapped in the lattice and other non-radiative decay processes occur. Moreover, we do not observe resonance of Raman intensity near room temperature, and we infer that F-centres do not contribute to resonant Raman scattering.

In the case of doped YSZ samples, the luminescence is much weaker than that of monoclinic zirconia. Foreign ion impurities are responsible for the low fluorescence intensity at 355 nm, but these impurities present very low concentration and should not contribute to the resonance. More interesting is the luminescence observed at room temperature under 266 nm excitation. The recombination of electrons and holes is around 500 nm (2.5 eV) in cubic zirconia and slightly lower in t' zirconia and it may explain the luminescence spectra observed. They correspond to energy level within the band gap. Among the defects, oxygen vacancies with yttria alloying in YSZ samples are most probable involved defects [petrik1999]. These defects within the band gap of YSZ are observed in optical and electronic spectroscopy by an Urbach tail [Camagni1992], [llopis1990], [wiemhofer1992]. The energy levels of oxygen vacancies are localized states below the conduction band edge, and they absorb light at lower energy than the band gap (theoretical study of Youssef and al. [youssef2012]). Their activation energy may correspond to the 2.7-3 eV as observed in our samples and by Petrik et al. [petrik1999]. The thermal activation of these defects is obviously participating in the high-temperature conductivity of YSZ [ikeda1985]. Moreover, some authors suggest a change in oxygen stoichiometry at high temperature [morell1997]. These defects in YSZ may affect the laser absorption. However, it seems that they do not contribute to the resonant scattering. The absorption is mainly composed of two contributions, defect absorption below the band gap and absorption due to the crossover of the (indirect) gap with the laser excitation line at 355 nm. This later effect is related to the resonance Raman scattering observed for the different compositions of samples at high temperature.

Temperature spectra of YSZ

The change of UV Raman spectra of m-ZrO_2, TBC, YSZ(111) and 38%YSZ samples as a function of temperature are presented in Figure A2a to d. For clarity, the spectra were vertically shifted, and only the contribution of the black body radiation without laser excitation was shown at the temperature of 1500 °C. In the case of m-ZrO_2 specimen (Figure 4a), the fluorescence in the background (discussed below) quenches at high temperature. An abrupt change in the number of Raman modes appeared around 1200 °C indicating a phase transition from monoclinic to tetragonal phase [ishigame1977], [perry1990]. TBC, YSZ(111) and 38%YSZ (Figure A2b to d) does not show phase transition with the change of temperature. One can note that high-temperature Raman spectra of TBC is still tetragonal but is very similar to cubic zirconia due to the strong broadening of modes (Figure A2d). The main observation of Figure A2 (a to d) is that Raman spectra are the persistent at high temperature in the four samples.

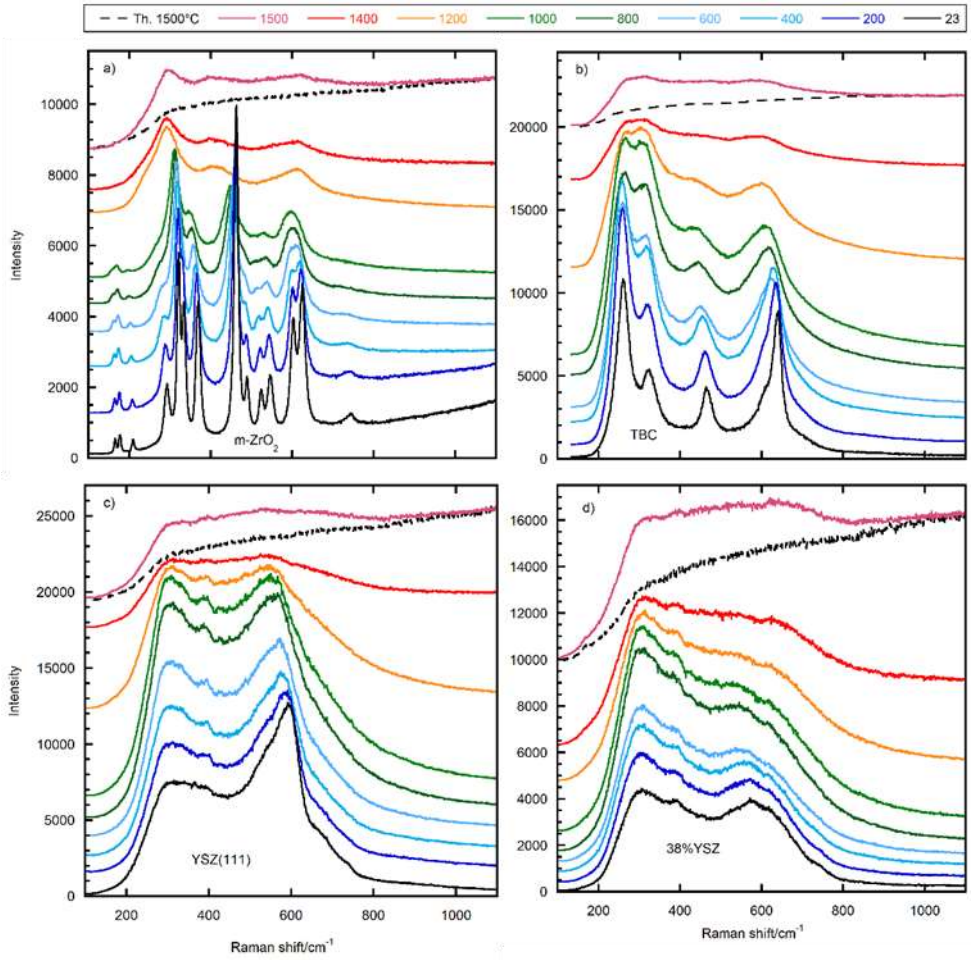

FIGURE A2 Raman spectra of m-ZrO_2, TBC, YSZ(111) and 38%YSZ as a function of temperature. The intensities are uncorrected, but spectra are shifted along the intensity axis for clarity. The thermal emission without laser at 1500 °C "Th 1500 °C" is given for comparison.

Complementary measurements in photoluminescence and Raman scattering were carefully measured with a step of 25 °C from room temperature to 900 °C in monoclinic zirconia in figure A3. Below 400 °C, the transmission is related to F-centre absorption that quenches in temperature. Consequently, the room temperature Raman intensity excited at 355 nm shows an underestimated by about 40% due to laser absorption. This effect disappears above 300–400°C. In figure A4, a zoom on the 355 nm laser absorption near the martensitic phase is presented. A clear hysteresis of the transition temperature is observed upon heating and cooling by a sudden increase of transmission up to 20%. Meanwhile, outside the transition, the intensity is in-line with the general trend of decay with temperature due to absorption closer and closer to the band gap. Still the sample is far from the crossover with the band gap and only a pre-resonance is observed.

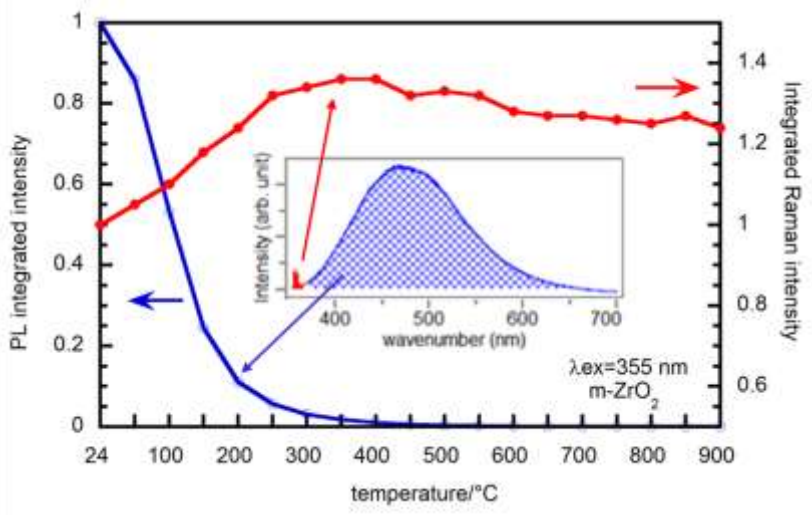

FIGURE A3 Integrated Raman intensity and photoluminescence intensity of m-ZrO_2 from RT to 900 °C The RT spectrum of Raman with photoluminescence of F-centres are given in the inset.